Bulletin of the Mineral Research and Exploration

http://bulletin.mta.gov.tr

2D inverse modeling of the gravity field due to a chromite deposit using the Marquardt's algorithm and forced neural network

Ata ESHAGHZADEH*[a], Sanaz SEYEDI SAHEBARI[b] and Alireza DEHGHANPOUR[c]

[a]*Danesh Tadbir Zima Institute, Chaloos, Iran*
[b]*Roshdiyeh Higher Education Institute, Tabriz, Iran.*
[c]*Islamic Azad University, Science and Research Branch, Tehran, Iran.*

Research Article

Keywords:
Chromite deposit, Finite vertical cylinder, Forced Neural Networks, Gravity, Marquardt's algorithm.

ABSTRACT

In this paper, two modeling method are employed. First, a method based on the Marquardt's algorithm is presented to invert the gravity anomaly due to a finite vertical cylinder source. The inversion outputs are the depth to top and bottom, and radius parameters. Second, Forced Neural Networks (FNN) for interpreting the gravity field as try to fit the computed gravity in accordance with the estimated subsurface density distribution to the observed gravity. To evaluate the ability of the methods, those are employed for analyzing the gravity anomalies from assumed models with different initial parameters as the satisfactory results were achieved. We have also applied these approaches for inverse modeling the gravity anomaly due to a Chromite deposit mass, situated east of Sabzevar, Iran. The interpretation of the real gravity data using both methods yielded almost the same results.

Received Date: 20.09.2018
Accepted Date: 20.01.2019

1. Introduction

Non-uniqueness is a common problem in the inverse modeling of the residual gravity anomaly. IT can assign a set of the measured gravity field data on the ground to the geometrical distributions of the subsurface mass with various shapes or physical parameters such as density and depth. One way to eliminate this ambiguity is to put a suitable geometry to the anomalous body with a known density followed by inversion of gravity anomalies (Chakravarthi and Sundararajan, 2004). Although simple models may not be geologically realistic, they are usually are sufficient to analyze sources of many isolated anomalies (Abdelrahman and El-Araby, 1993*a.b*). The interpretation of such an anomaly aims essentially to estimate the parameters such as shape, depth, and radius of the gravity anomaly causative body such as geological structures, mineral mass and artificial subsurface structures.

Several graphical and numerical methods have been developed for analyzing residual gravity anomalies caused by simple bodies, such as Saxov and Nygaard (1953) and Bowin et al. (1986). The methods include, for example, Fourier transform (Odegard and Berg, 1965; Sharma and Geldart,1968); Mellin transform (Mohan et al., 1986); Walsh transforms techniques (Shaw and Agarwal, 1990); ratio techniques (Hammer, 1974; Abdelrahman et al., 1989); least-squares minimization approaches (Gupta, 1983; Lines and Treitel, 1984; Abdelrahman, 1990; Abdelrahman

Citation Info: Eshaghzadeh, A., Sahebari, A.S., Dehghanpour, A. 2020. 2D inverse modeling of the gravity field due to a chromite deposit using the Marquardt's algorithm and forced neural network. Bulletin of the Mineral Research and Exploration, 161, 33-47. https://doi.org/10.19111/bulletinofmre.589224

* *Corresponding author: Ata ESHAGHZADEH, eshagh@alumni.ut.ac.ir*

et al., 1991) and different neural networks (Eslam et al., 2001; Osman et al., 2006, 2007; Al-Garni, 2013; Eshaghzadeh and Kalantari, 2015; Eshaghzadeh and Hajian, 2018); effective quantitative interpretations using the least-squares method (Gupta, 1983) based on the analytical expression of simple moving average residual gravity anomalies are yet to be developed. The moving average method has mostly used for interpreting the potential fields (Abdelrahman et al., 2003; Abdelrahman et al., 2015; Abdelrahman and Essa, 2015). Abdelrahman and El-Araby (1993*a, b*) introduced an interpretive technique based on fitting simple models convolved with the same moving average filter as applied to the measured gravity. A simple method proposed by Essa (2007) is used to determine the depth and shape factor of simple shapes from residual gravity anomalies along the profile. Another automatic method, the least-squares method, was proposed by Asfahani and Tlas (2008), by which the depth and amplitude coefficient can be determined.

Nowadays Artificial Neural Networks (ANNs) are of main research concern, so that involving researchers of various disciplines and sciences. Topics contributing to this investigation contain biology, computing, electronics, mathematics, medicine, geophysics and etc (Bichsel, 2005). The new method, the artificial neural network, has been employed in recent years for different branch of geophysics especially potential fields. For example, the situation of buried steel drums as magnetic dipole source is evaluated using supervised artificial neural network (Salem et al., 2001). Eslam et al., (2001) specified depth and radius of subsurface cavities from microgravity data using back propagation neural networks. Hajian (2004) estimated depth and shape factor of the gravity anomaly source by applying Feed-Forward Back-Propagation Neural Networks. Chua and Yang (1998) defined a new approach in neural networks titled Cellular Neural Network (CNN), which is focused on 2D image processing. CNN was applied for separation of regional/residual potential sources in geophysics (Albora et al., 2001*a*, *b*). Forced Neural Networks for gravity anomaly analysis was proposed by Osman et al. (2006; 2007). Abedi et al. (2009) calculated the depth and radius of the simple geometry by the neural network from the gravity anomalies. Kaftan et al. (2011) applied Artificial Neural Network for evaluating Seferihisar geothermal area by the gravity data. Al-Garni (2013) used MNN inversion for estimating the depth of the gravity anomaly source related to simple geometry such as sphere, infinite horizontal cylinder and semi-infinite vertical cylinder. Eshaghzadeh and Kalantari (2015) have been proposed a new method based on feed-forward neural network for gravity field inverse modeling due to anticlinal structures. Eshaghzadeh and Hajian (2018) have introduced a new concept of the modularity for analysis the gravity field by modular neural network.

In this paper, a simultaneous non-linear inversion based on Marquardt optimization is developed to estimate the radius and depth to top and bottom parameters of a structure similar to the finite vertical cylinder. The Marquardt inversion method has been used for modeling the geological structures such as faulted beds (Chakravarthi and Sundararajan, 2005), anticlinal and synclinal structures (Chakravarthi and Sundararajan, 2007; 2008), multiple prismatic structures (Chakravarthi and Sundararajan, 2006). We also employ Forced Neural Networks (FNN) introduced by Osman et al. (2006; 2007) as a comparative method. The validity of the methods are tested on synthetic gravity data with and without random noise and also on a real gravity data set from Iran. Furthermore, the Euler deconvolution method is utilized to verify the estimated depths to top by the presented methods.

2. Forward Gravity Modeling

The gravity effects of a finite vertical cylinder is defined by Hammer (1974)

$$g(x) = KF(x) \qquad \text{(equation 1)}$$

Where k is amplitude coefficient as

$$F(x_i)=\frac{1}{\sqrt{x^2+z^2}}-\frac{1}{\sqrt{x^2+h^2}},\ K=\pi G\rho R^2 \qquad \text{(equation 2)}$$

where x is the horizontal location coordinate of measurement points, z and h represent the depths to the top and base planes of causative structure from ground surface respectively, G is the gravitational constant, R is the radius of the horizontal cross section of a vertical cylinder, and ρ is the density contrast (Figure 1).

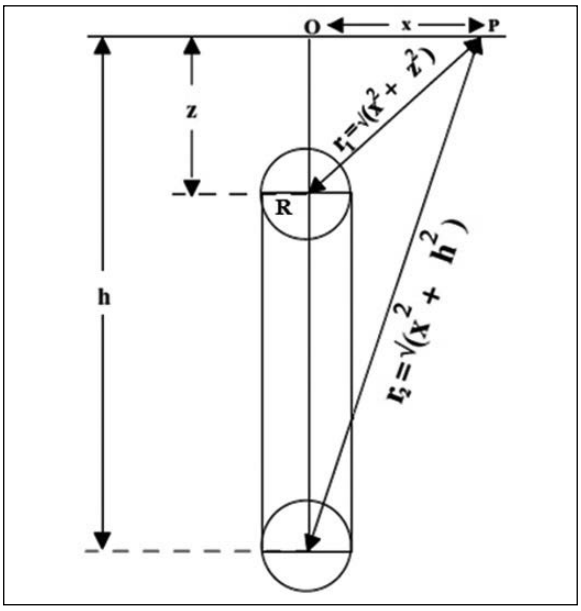

Figure 1- Geometries of the finite vertical cylinder.

3. Marquardt Method

The inversion of gravity anomalies is implicitly a mathematical process, trying to fit the computed gravity anomalies to the observed ones in the least-squares approach and then estimating the three parameters of the finite vertical cylinder model namely depth to top (z), depth to bottom (h) and radius (R). The process of the inversion begins with computing the theoretical gravity anomaly of the simple geometry using equation (1).

The difference between the observed gravity $g_{obs}(x_i)$, and calculated gravity anomaly of an initial assumed model $g_{cal}(x_i)$, can be estimated by a misfit function, J (Chakravarthi and Sundararajan, 2007), as

$$J=\sum_{i=1}^{N}[g_{obs}(x_i)-g_{cal}(x_i)]^2 \qquad \text{(equation 3)}$$

N is the number of observed gravity data. We have employed the Marquardt's algorithm (Marquardt, 1963) given by Chakravarthi and Sundararajan (2006) for minimizing the misfit function until the normal equations can be solved for over all modifications of the three unknowns structural parameters, i.e. depth to top (z), depth to bottom (h) and radius (R), as

$$\sum_{i=1}^{N}\sum_{k=1}^{2}\frac{\partial g(x_i)}{\partial a_j}\frac{\partial g(x_i)}{\partial a_k}(1+\delta\lambda)da_k = \sum_{i=1}^{N}[g_{obs}(x_i)-g_{cal}(x_i)]\frac{\partial g(x_i)}{\partial a_j},\ for\ \ j=1,2,3 \qquad \text{(equation 4)}$$

where da_k, k=1, 2 and 3 are the amendments to the three model parameters of the simple geometry structure, i.e. radius, depth to top and bottom. Also,

$$\delta=\begin{cases}1\ for\ \ k=j,\\ 0\ for\ \ k\neq j,\end{cases}$$

and λ is the damping factor. The advancements, da_k, k=1, 2 and 3 evaluated from equation (4) are then added to or subtracted from the available parameters estimated from last iteration and the process repeats until the misfit, J, in equation (3) descends below a predetermined allowable error or the damping factor obtains a large value which is greater than predefined amount or the repetition continues until the end of the considered number for iterations (Chakravarthi and Sundararajan, 2008).

Partial derivatives required in the normal system of equation (4) are calculated numerically by the relations derived from equation (1) considering to each parameter to be solved. The Partial derivatives of the finite vertical cylinder source than the three shape parameters, namely radius, depth to top and depth to bottom can be computed, respectively, as

$$\frac{\partial g}{\partial R}=\pi G\rho R\left[\frac{1}{\sqrt{x^2+z^2}}-\frac{1}{\sqrt{x^2+h^2}}\right] \qquad \text{(equation 5)}$$

$$\frac{\partial g}{\partial z}=\pi G\rho R^2 z\left[\frac{1}{\left(x^2+z^2\right)^{3/2}}\right] \qquad \text{(equation 6)}$$

$$\frac{\partial g}{\partial h}=\pi G\rho R^2 h\left[\frac{1}{\left(x^2+h^2\right)^{3/2}}\right] \qquad \text{(equation 7)}$$

3.1. Theoretical Model Evaluation by Marquardt Method

Figure 2a shows the observed and calculated gravity field variations with 1 m interval along a 100 m profile due to an initial finite vertical cylinder model with the parameters z=30 m, h=60 m and R=10 m and an assumed finite vertical cylinder model with parameters z=27 m, h=64 m and R=8 m (Figure 2b) where the maximum gravity is the center of the profile. The density contrast is given as Δρ=1000 kg/m^3. Hence, the assumed parameters and observed gravity field related to the initial model are the inputs to the inversion algorithm which coded in Matlab. During inversion, Δρ is constant and the model

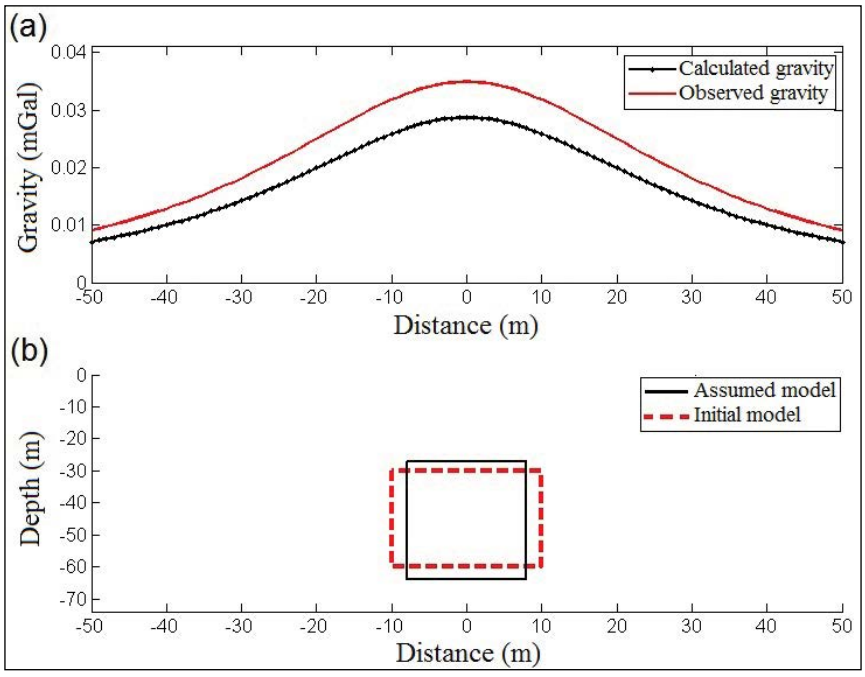

Figure 2- a) Observed and calculated gravity due to b) initial and assumed finite vertical cylinder models.

parameters, z, h and R are improved iteratively. The predefined values for error or misfit (J), iteration and damping factor (λ) are 0.00000001 mGal, 20 and 15, respectively. The initial damping factor is 0.5.

The misfit, J, reduces intensely from its initial value of 0.0021 mGal at the first iteration to 0.000042 mGal at the end of the 3rd iteration and then gradually reaches zero after the 16th iteration which is smaller than the allowable error value (Figure 3d). The

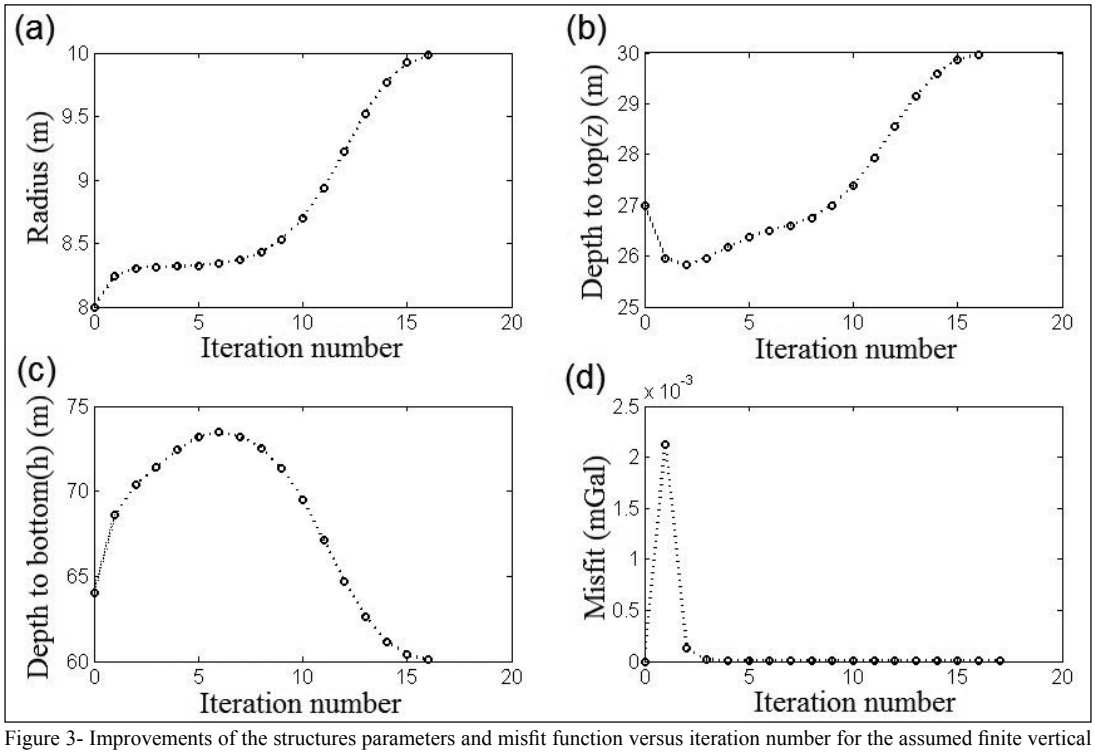

Figure 3- Improvements of the structures parameters and misfit function versus iteration number for the assumed finite vertical cylinder model in figure 2.

iteration terminated at 16th echo and therefore the estimated parameters at 16th iteration are the final results of the inversion.

Figures 3a, 3b and 3d illustrate the variations of the model parameters R, z and h during inversion with increasing the iteration number. The conclusive obtained parameters values are z=30 m, h=60 m and R=10 m. Figure 4a shows the computed gravity anomaly from the inferred structure which is shown in figure 4b as is completely similar initial model.

The efficacy of error has been evaluated by adding 10% random noise to the gravity response of the initial finite vertical cylinder model (Figure 5a) using the following expression:

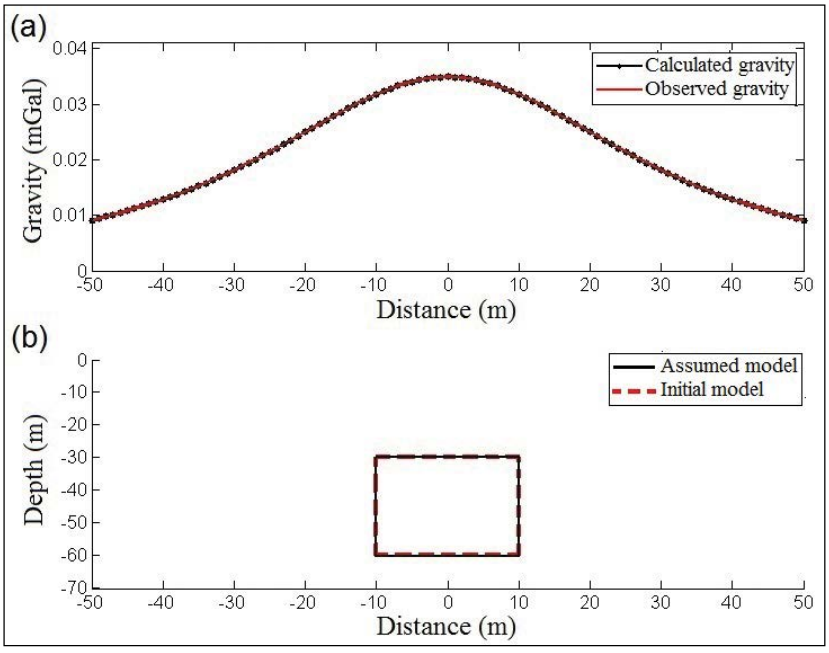

Figure 4- a) Observed and calculated gravity due to b) initial and estimated finite vertical cylinder model.

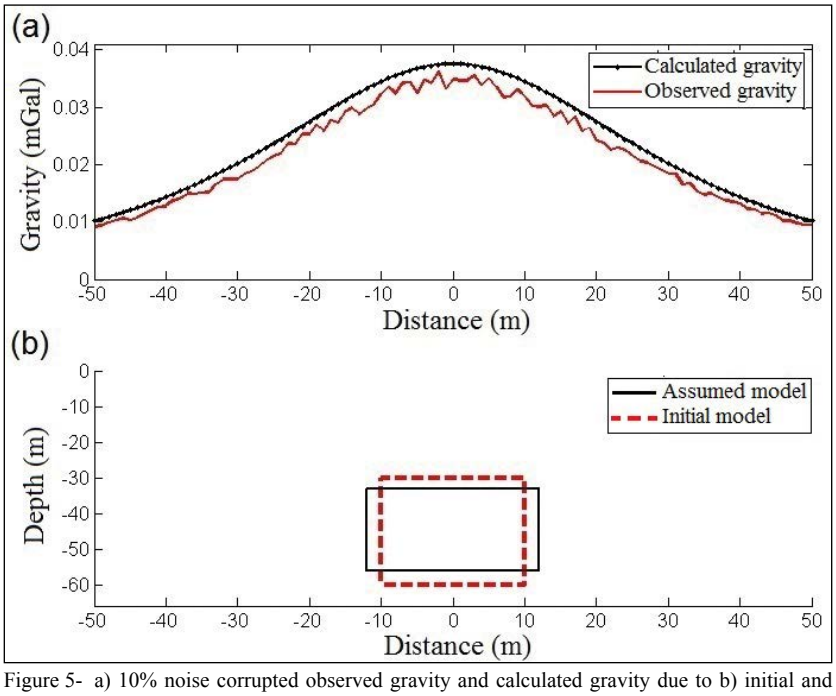

Figure 5- a) 10% noise corrupted observed gravity and calculated gravity due to b) initial and assumed finite vertical cylinder models.

$g_{nois}(x_i)=g_{obs}(x_i)[1+(RAN(i)-0.5)x0.1]$ (equation 8)

where $g_{nois}(x_i)$ is the noise corrupted synthetic data at x_i, and RND (i) is a pseudorandom number whose range is between 0 to 1.

The initial values for the parameters of the assumed finite vertical cylinder model are given as z=33 m, h=56 m and R=12 m (Figure 5b). The predefined values for error or misfit (J), iteration and damping factor (λ) are 0.00001 mGal, 100 and 15, respectively. The initial damping factor is 0.2. The misfit, J, reduces quickly from its initial value of 0.00051 mGal at the first iteration to 0.000049 mGal at the end of the 3th iteration and then incrementally attains 0.000042 mGal after the 32th iteration and this value remain constant to latest iteration (Figure 6d). The final evaluated values for the depth to top (z), depth to bottom (h) and radius (R) are 30.26 m, 60.04 and 10.06 m, respectively (Figure 6b, 6c and 6d). The percentage of error in the estimation of the model parameters, that is, z, h and R are about 0.87, 0.07 and 0.6 m, respectively.

Figure 7a shows the generated gravity anomaly of the final structure that is derived from the estimated parameters as shown in Figure 7b. The numerical results obtained from the interpretation of the synthetic gravity data, with and without random noise, are tabulated in table 1.

For evaluating the convergence of the Marquardt inversion, two different initial horizontal cylinder models were assumed to consider the gravity anomalies related to them with and without a random noise (Table 2). The estimated structural parameters approximately mimic the supposed ones.

Table 1- Numerical results evaluated from the initial and assumed structural parameters for the finite vertical cylinder model, with and without added noise.

Case	**Without noise**			**With noise**		
Parameter	**z (m)**	**h (m)**	**R (m)**	**z (m)**	**h (m)**	**R (m)**
Initial	30	60	10	30	60	10
Assumed	27	64	8	33	56	12
Estimated	30	60	10	30,26	60,04	10,06
Error %	0	0	0	0,87	0,07	0,6

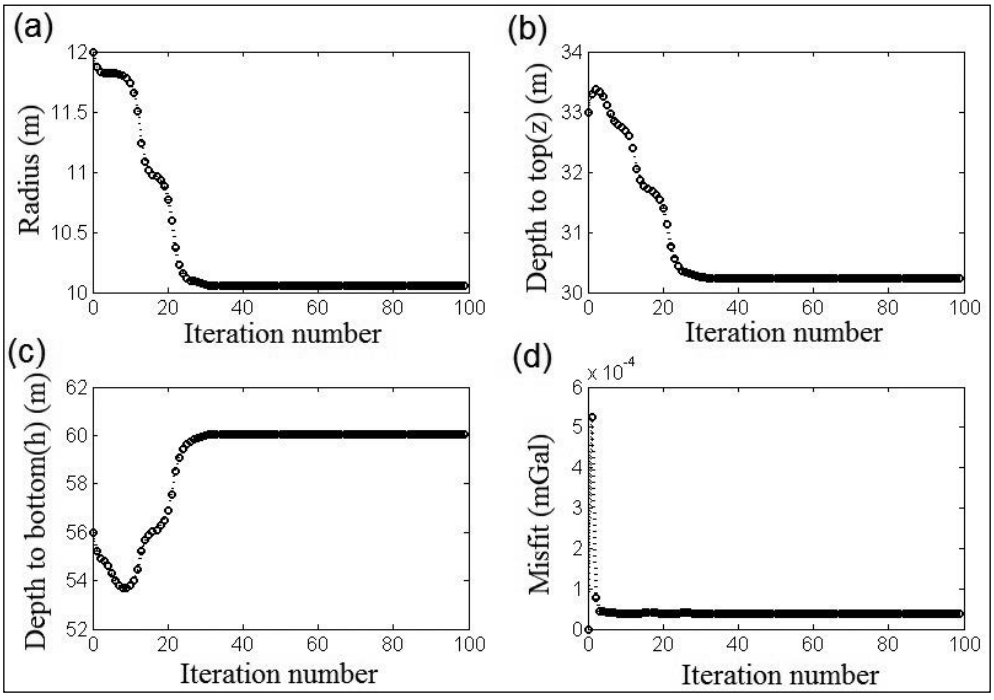

Figure 6- Improvements of the structures parameters and misfit function versus iteration number for the assumed finite vertical cylinder model in figure 5.

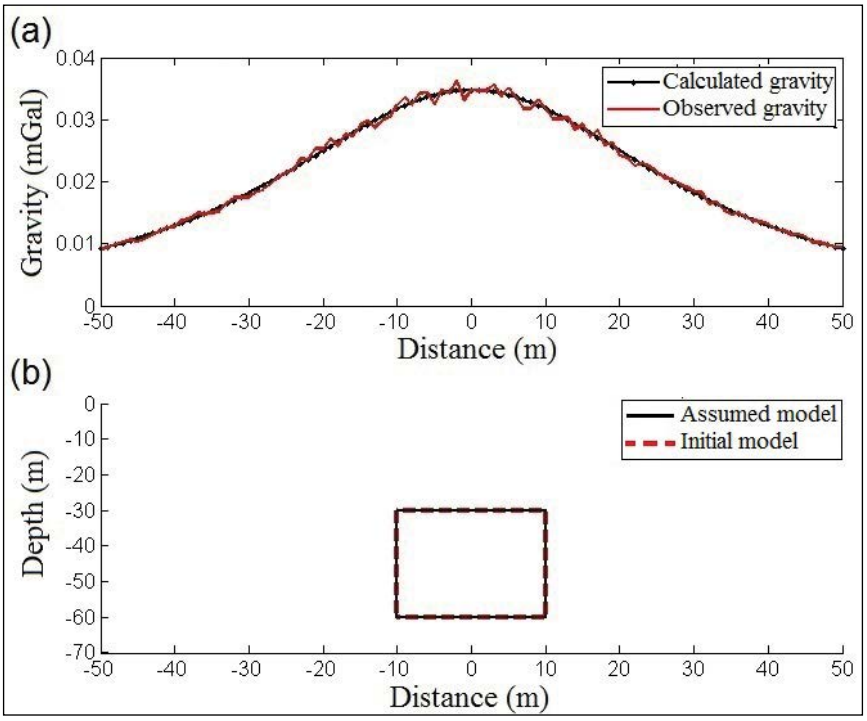

Figure 7- a) 10% noise corrupted observed gravity and calculated gravity due to, b) initial and estimated finite vertical cylinder models.

Table 2- Numerical results evaluated from the gravity responses of the two different finite vertical cylinder models. To model 1 and model 2 have been added 10% and 15% random noise, respectively.

		Model 1			Model 2		
Parameter		**z (m)**	**h (m)**	**R (m)**	**z (m)**	**h (m)**	**R (m)**
Initial		12	70	15	40	85	20
Assumed		16	65	11	34	78	16,5
Estimated	**Without noise**	12,02	70	14,99	40	85,02	20,01
	Error%	0,17	0	0,067	0	0,023	0,05
	With noise	11,94	70,8	15,11	39,1	86,5	18,9
	Error%	0,5	1,14	0,73	2,25	1,76	5,5

4. Forced Neural Network

In this study, we employ the Forced Neural Network (FNN) introduced by Osman et al. (2006, 2007) to determine the shape and density contrast of the target using the gravity anomaly as is assumed which the underground mass has been composed from the juxtaposed prisms.

FNN architecture is manufactured of several simple processing elements commonly known as neurons, which are connected together and performance in parallel (Figure 8). To estimate the efficient values of inputs and outputs, the various weights during the learning are attributed to these connections as these weights are multiplied by effective values of inputs and outputs (Osman et al. 2007). The primary objective of neural networks is to find out such weights that present the best output. Back propagation is one of the most well-known learning algorithms for neural networks.

In this approach, we need to compute the gravity anomaly due to a prismatic structure. There are some techniques for calculating the gravitational attraction of two-dimensional prism shaped masses, such as Talwani and Ewing (1960), Bhattacharyya (1964), Talwani (1965), Nagy (1966), Plouff (1976), Last and Kubik (1983) and Gerkens (1989). We apply the 2D prism equation developed by Last and Kubik (1983) to

estimate the gravity anomaly at point p because of any block located at (i,j) coordinates, which is given as

$$g_{pij} = 2G\Delta\rho\left[\begin{array}{l}(x_i - x + \frac{d}{2})\log(\frac{r_2 r_3}{r_1 r_4}) + d\log(\frac{r_4}{r_3}) - \\ (z_j + \frac{h}{2})(\theta_4 - \theta_2) + (z_j - \frac{h}{2})(\theta_3 - \theta_1)\end{array}\right], \text{(equation 9)}$$

where

$$r_1^2 = (z_j - \frac{h}{2})^2 + (x_i - x + \frac{d}{2})^2,$$

$$r_2^2 = (z_j + \frac{h}{2})^2 + (x_i - x + \frac{d}{2})^2,$$

$$r_3^2 = (z_j - \frac{h}{2})^2 + (x_i - x - \frac{d}{2})^2,$$

$$r_4^2 = (z_j + \frac{h}{2})^2 + (x_i - x - \frac{d}{2})^2,$$

and

$$\theta_1 = \tan^{-1}(x_i - x + \frac{d}{2})/(z_j - \frac{h}{2}),$$

$$\theta_2 = \tan^{-1}(x_i - x + \frac{d}{2})/(z_j + \frac{h}{2}),$$

$$\theta_3 = \tan^{-1}(x_i - x - \frac{d}{2})/(z_j - \frac{h}{2}),$$

$$\theta_4 = \tan^{-1}(x_i - x - \frac{d}{2})/(z_j - \frac{h}{2}),$$

Here G is the gravitational constant, $\Delta\rho$ is density contrast, d and h are the width and height of the each block, x_i and z_j indicate the coordinate of the each block. The equation (9) can be rewritten as

$$g_p = \sum_{h=0}^{i}\sum_{k=0}^{j}\Delta\rho_{hk} \times W_{phk} \qquad \text{(equation 10)}$$

Thus, there are i rows and j columns. By noting to the equation 10 can find that $\Delta\rho_{hk}$ are the weights of the neuron, i.e. each pixel and during the back propagation, the weights are updated and the output of the neuron exhibits the gravity anomaly (Figure 8). Hence, the density contrast are obtained. It is worth noting that in this method, from the linear activation function is used.

Because non-uniqueness in the responses, the results obtained from the FNN do not demonstrate the exact distribution of the structure. To model the causative mass correctly, a filter must serve until the value of the $\Delta\rho$ which is very close to the zero, corresponding to the density contrast which is obtained from geological features of the region under investigation, assign as zero, otherwise the value of $\Delta\rho$ is set to the density contrast of the geological region after back propagation (Osman et al., 2007). For obtaining more details, see Osman et al. (2006; 2007).

4.1 Theoretical Model Evaluation by FNN

Figure 9a displays the observed gravity related to a synthetic model assuming the density contrast 500 kg/m^3 in which the depth to top of the model is 2 m, depth to bottom is 10 m, the width of the upper part and lower part is 3 m, while the middle part is 9 m, as shown in figure 9b.

The gravity anomalies of this model are considered as input data to the FNN, then, shape, location, and density contrast parameters of the buried structure are estimated using trained FNN, as after adequate iteration is applied, constant values are assigned to the output of the neuron according to the density difference $\Delta\rho$, and this process is continued until the mean square error of the output, g_p which is shown in figure 8, becomes sufficiently little.

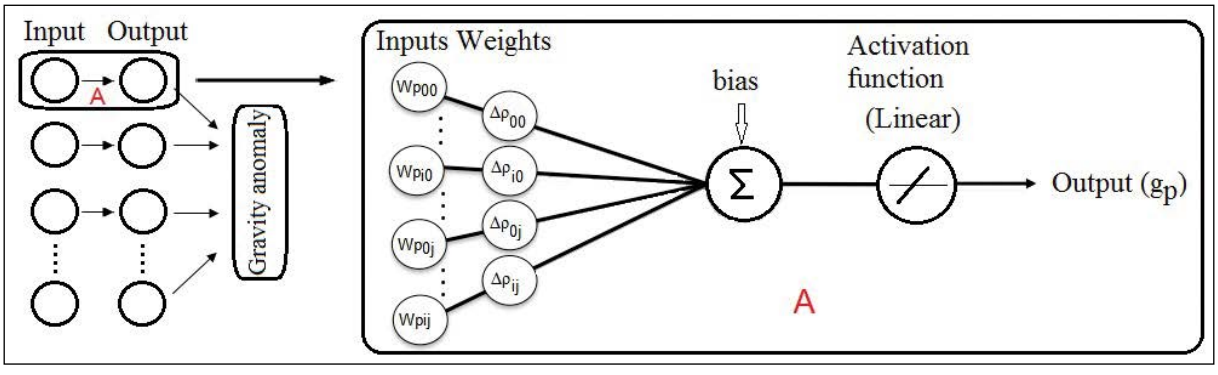

Figure 8- Sketch of the Forced Neural Network (FNN) architecture for gravity anomaly.

Figure 9c shows the evaluated structure by FNN which from the density contrast, shape and position points of view is similar the assumed one. The inverted gravity from FNN is illustrated in figure 9a.

5. Real Gravity Field Analysis

The site under survey is located in the east of Iran, around Sabzevar. The outcomes of the stones in the this area are mostly the alkali and ultrabasic igneous rocks and Ophiolite as the Chromite mineralization can be found in these rocks (Figure 10). In this region, the Chromite deposits are massive. Figure 11 shows the Bouguer gravity anomalies map of the area under consideration. The gravity measurement was done along 12 profiles with a station interval of about 10 m. The gravity data covering a 120×100 m area of the exploration region in Sabzevar.

For reaching to the residual gravity anomalies which is our desire, the regional gravity anomalies must be removed using a trend (degree two polynomial) from the Bouguer anomaly. Figure 12 displays the map of the computed local gravity field. The host rock of the chromite have the positive density contrast than the surrounding formation, therefore on the residual gravity anomalies map is appeared as the positive anomaly. The average density of the Chromite mass is about 4.5 gr/cm^3, whereas the density of the encompassing formation is between 3 gr/cm^3 to 3.5 gr/cm^3. Here, we analyze the residual gravity field variations along the profile AA′ which runs across the Chromite mineral mass in an approximately W–E direction as is shown in figure 12. The length of profile is 42 m and the gravity sampling interval is given as 2 m.

We applied the Marquardt inversion for the real gravity data where the causative mass shape was assumed as a finite vertical cylinder. The observed gravity field variations along profile AA′ is demonstrated in figure 13a. The initial values of the depth to top and bottom and radius parameters are given as z=8.5 m, h=80 m and R=11 m (Figure 13b). The density difference is chosen as 1500 kg/m^3. The

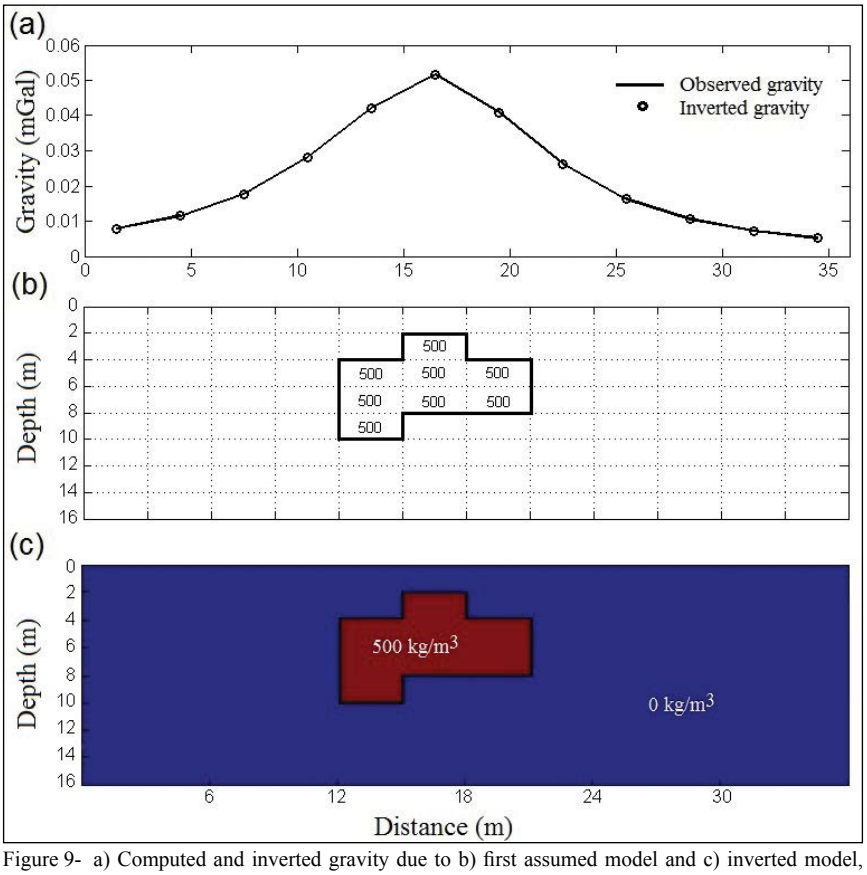

Figure 9- a) Computed and inverted gravity due to b) first assumed model and c) inverted model, respectively.

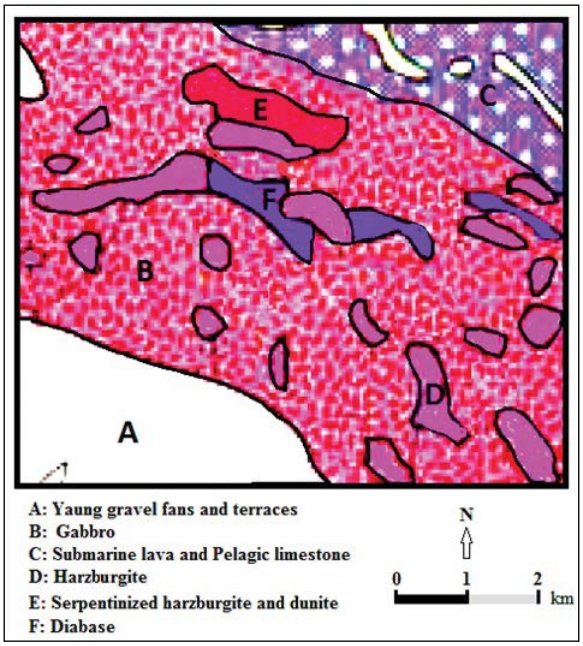

Figure 10- The geological map of the region under investigation.

gravity anomaly produced by the presumed initial values is represented in figure 13a. The assigned values for misfit (J), iteration and damping factor (λ) are 0.001 mGal, 50 and 20, respectively. The variability of each shape parameter and misfit of the finite vertical cylinder geometry model against the iteration number during inversion process is shown in figure 14.

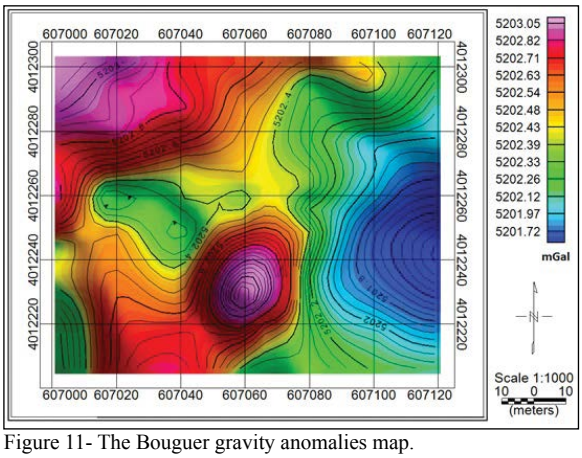

Figure 11- The Bouguer gravity anomalies map.

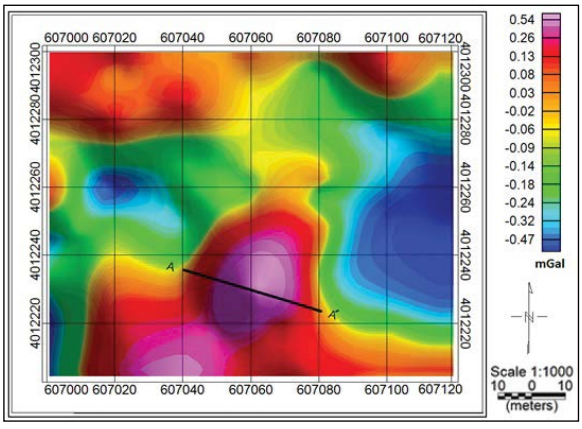

Figure 12-The residual gravity anomalies map. The profile AA′ is specified with a nearly W-E direction.

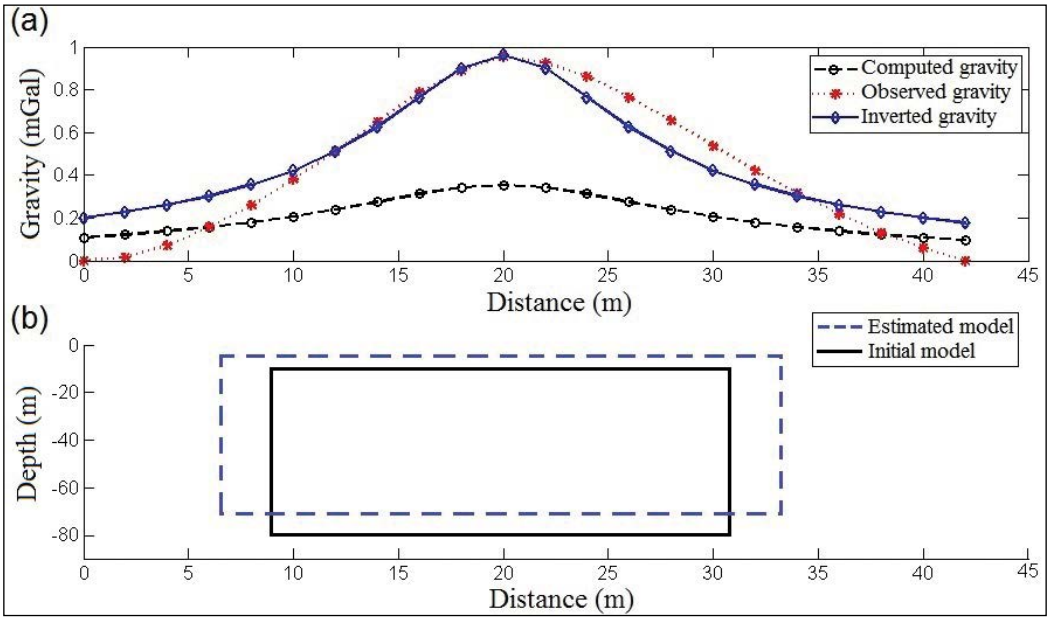

Figure 13- a) Observed gravity along profile AA′, calculated and inverted gravity due to b) initial and estimated finite vertical cylinder models.

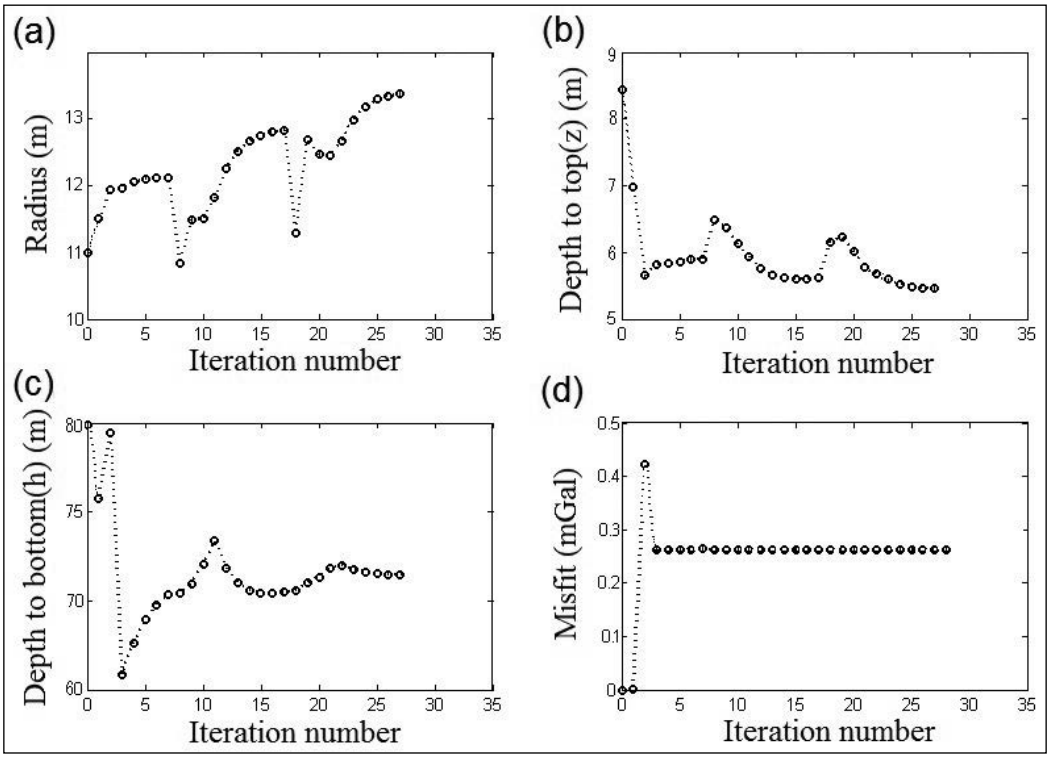

Figure 14- The variations of a) Radius b) depth to top c) depth to bottom d) misfit function versus iteration number for the real gravity data.

The performed iteration is 27, before it was ceased, as in the end of this iteration number, the damping factor obtained a value greater than the predefined value. The misfit abided constant after the 3th iteration while three other parameters have changed with each iteration as in the 27th iteration have been obtained the amounts 5.4 m, 72 m and 13.5 m for the depth to top, depth to bottom and radius, respectively. The inverted gravity due to the estimated parameters is brought in figure 13a whereas the inferred structure is shown in figure 13b. The assumed and inverted structural parameters are given in table 3.

Table 3- Numerical results evaluated from the real gravity data.

Parameter	**z (m)**	**h (m)**	**R (m)**	**z (m)**	**h (m)**	**R (m)**
Assumed	8,5	80	11	4	65	16
Estimated	5,4	72	13,5	5,45	71,8	13,6
Iteration	27			43		
Misfit (mGal)	0,265			0,0057		

The permanency and isotropy of the interpreted parameters from the real gravity data was investigated using different assumed values (Table 3). The estimated structural parameters illustrate a very slight differences that confirm the stability of the method.

The gravity profile AA′ in residual anomaly map is also analyzed for modeling with FNN approach. The length and width of each block was considered as 5 m and 10 m, respectively. To achieve a under surface model as a finely detailed map, the evaluated density distribution was interpolated, where figure 15 illustrate the estimated structure for the Chromite deposit mass based on the density contrast distribution. The central part of the modeled deposit have a density contrast of 1600 kg/m^3 and getting away from the center, this value slake as expected. By considering the inverted structure by FNN, the depth to top and bottom and radius parameters of the buried mass can consider as about 8 m, 70 m and 9 m, respectively.

For comparison, the generated gravity according to the interpreted mass using FNN and Marquardt inversion and also real gravity have been shown in figure 16. We have applied the standard error (SE) as a

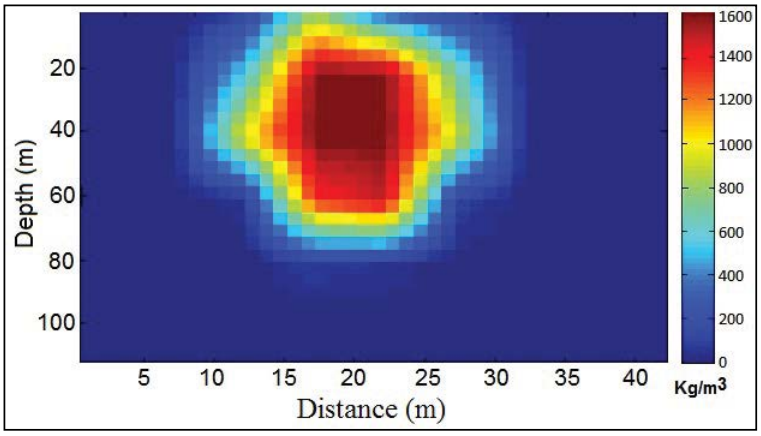

Figure 15- The inverted density distribution from analyzing the real gravity data using FNN.

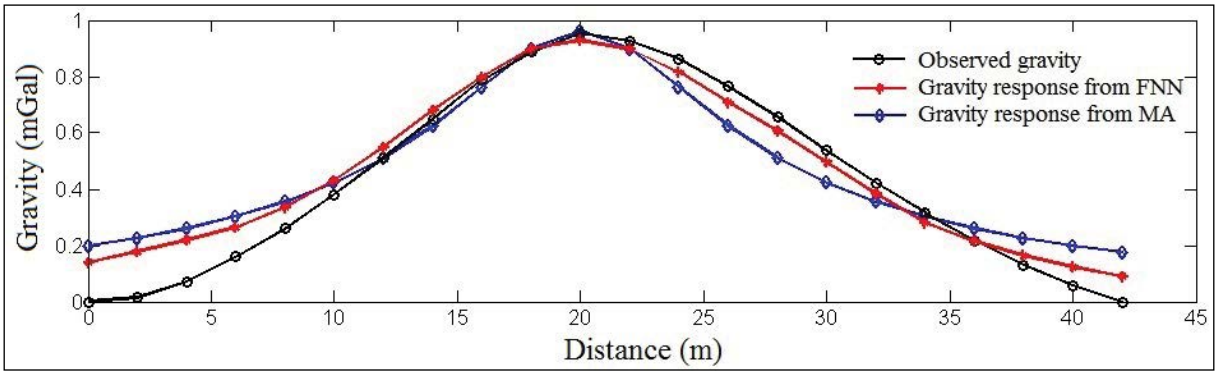

Figure 16- The observed gravity and gravity responses obtained from the FNN and Marquardt inversion (MA).

criteria in order to compare the observed and evaluated gravity values (Asfahani and Tlas, 2008):

$$SE = \sqrt{\frac{\sum_{i=1}^{N}\left[g_o(x_i) - g_c(x_i)\right]^2}{N}} \qquad \text{(equation 11)}$$

where g_o and g_c (i = 1, ..., N) are the observed and the evaluated values at the points x_i (i = 1, ..., N), respectively. The standard error for the FNN and Marquardt's algorithm methods are 0.09 and 0.126 mGal, respectively. Therefore, according to the computed SE, the inverted structure from FNN are closer to reality.

The Euler deconvolution method is a popular and well known technique in potential fields study which is widely used for estimating the depth of the anomaly source. In this study, we have employed the Euler method for calculating the depth of the Chromite mass by choosing a structure index of 1 and a window size of 5×5 points. Figure 17 show the solutions obtained from Euler deconvolution as plotted on the residual gravity anomaly map. The Euler solutions located on the gravity anomaly present a depth between 5 to 10 m for the buried deposit (red points in figure 17). Because the estimated depth to top by the all three methods are in a same range, thus, it was found that the introduced methods operate correctly. The attained results for the real gravity anomaly have been summarized in table 4.

Table 4- Evaluated parameters using the various methods.

	Parameters			
Methods	**z (m)**	**h (m)**	**R (m)**	**SE (mGal)**
FNN	8	70	9	0,09
Marquardt's algorithm	5,4	72	13,5	0,126
Euler	5-10	-	-	-

6. Conclusions

In this paper, we have introduced a optimization approach based on the Marquardt's algorithm and have also applied the Forced Neural Networks for the inverse modeling of the residual gravity anomaly due to the finite vertical cylinder geometric shape.

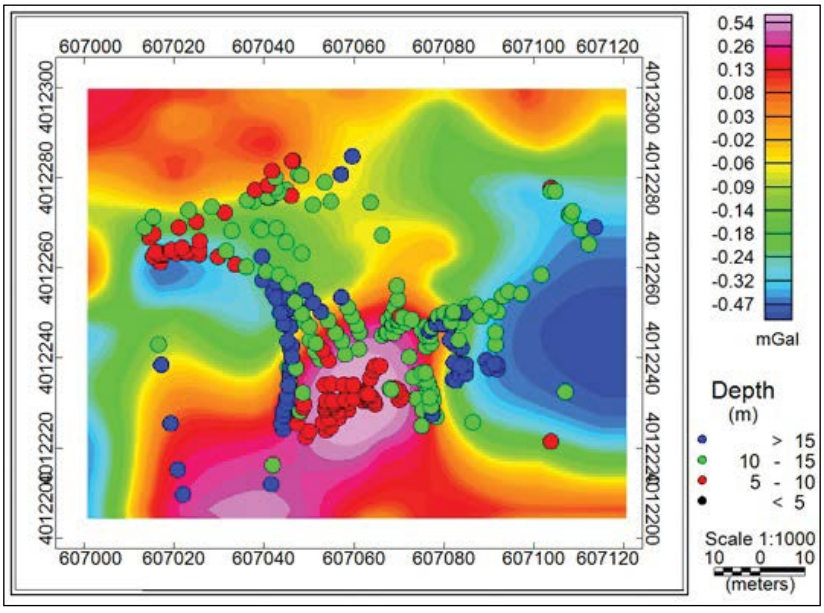

Figure 17- The depth solutions estimated by the Euler deconvolution method for the residual gravity anomalies.

To check the constancy and convergency of the parameters attained from the Marquardt inversion, the noise-free and noise corrupted theoretical gravity data related to the different initial models were used and it was eventuated that the inversion yields almost the same solutions in all cases. Moreover, the performance of the FNN was evaluated by the synthetic gravity data set. The stable and accurate solutions verify the reliability and applicability of the both Marquardt's algorithm and FNN methods as the powerful and useful inverse modeling tools.

The methods were used for estimating the buried structure parameters and determining the condition of the underground density distribution using the gravity anomaly of a Chromite deposit from Iran. The computed values for the depth to top, depth to bottom and radius parameters by the Marquardt inversion are 5.4 m, 72 m and 13.5 m, respectively and by the FNN method are about 8 m, 70 m and 9 m, respectively. Therefore, the acquired dimensions for the causative mass are very close and the inverted gravity from the final interpreted structure by these procedures conform to the real gravity along profile AA′ cross-section. The minimum standard error value was considered as a criterion for selecting the best mass shape, as the estimated parameters depict a acceptable structure naturally. As expected, the standard error amount between the inverted gravity from the FNN and real gravity is smaller than one between the inverted gravity from the Marquardt's algorithm and real gravity, because in reality a structure with invariable density whose feature be closely a geometric shape. In other words, the gravity causative mass has not a perfect geometry shape and is a heterogeneous body. In nonlinear inversion, we consider the gravity anomaly source as a regular geometry shape with a constant density, therefore we try to interpret the anomaly source with the most similar geometry shape where the error between the observed and computed gravity be least. Hence, existence of a mismatch between observed and computed data is unavoidable. Therefore, the estimated values for the depth to top (z), depth to bottom (h) and radius (R) parameters using the FNN are closer to the reality than those computed by the Marquardt inversion method. The evaluated depths to top have also good conformity with the Euler solutions.

References

Abdelrahman, E.M. 1990. Discussion on "A least-squares approach to depth determination from gravity data" by O. P. Gupta. Geophysics 55, 376-378.

Abdelrahman, E.M., El-Araby, T.M. 1993*a*. A least-squares minimization approach to depth determination from moving average residual gravity anomalies. Geophysics 58,1779–1784.

Abdelrahman, E.M., El-Araby, H.M. 1993*b*. Shape and depth solutions from gravity using correlation factors between successive least-squares residuals. Geophysics 59, 1785–1791.

Abdelrahman, E.M., Essa, K.S. 2015. A new method for depth and shape determinations from magnetic data. Pure and Applied Geophysics 172, 439–460.

Abdelrahman, E.M., Bayoumi, A.I., Abdelhady, Y.E., Gobashy, M.M., El-Araby, H.M. 1989. Gravity interpretation using correlation factors between successive least-squares residual anomalies. Geophysics 54, 1614-1621.

Abdelrahman, E.M., Bayoumi, A.I., El-Araby, H.M. 1991. A least-squares minimization approach to invert gravity data. Geophysics 56, 115-l 18.

Abdelrahman, E.M., El-Araby, T.M., Essa, K.S. 2003. A least-squares minimisation approach to depth, index parameter, and amplitude coefficient determination from magnetic anomalies due to thin dykes. Exploration Geophysics 34, 241–248.

Abdelrahman, E.M., Essa, K.S., El-Araby, T.M., Abo-Ezz, E.R. 2015. Depth and shape solutions from second moving average residual magnetic anomalies. Exploration Geophysics, 47/1, 58-66.

Abedi, M., Afshar, A., Ardestani, V.E., Norouzi, G.H., Lucas, C. 2009. Application of various methods for 2D inverse modeling of residual gravity anomalies. Acta Geophysica 58/2, 331-336.

Albora, A.M., Uçan, O.N., Özmen, A. 2001*a*. Residual separation of magnetic fields using a cellular neural network approach. Pure Appl Geophys,158,1797–1818.

Albora, A.M., Uçan, O.N., Özmen, A., Özkan, T. 2001*b*. Evaluation of Sivas-Divriği region Akdağ iron ore deposits using cellular neural network. J Appl Geophys 46,129–142.

Al-Garni, M.A. 2013. Inversion of residual gravity anomalies using neural network. Arab J Geosci 6, 1509–1516.

Asfahani, J., Tlas, M. 2008. An automatic method of direct interpretation of residual gravity anomaly profiles due to spheres and cylinders. Pure and Applied Geophysics 165/5, 981–994.

Bhattacharyya, B.K. 1964. Magnetic anomalies due to prism-shaped bodies with arbitrary polarization. Geophysics 29, 517–531.

Bichsel, M. 2005. Image processing with optimum neural networks. IEEE International Conference on Artificial Neural Networks, 513, IEEE, London, 374–377.

Bowin C., Scheer E., Smith W. 1986. Depth estimates from ratios of gravity, geoid, and gravity gradient anomalies. Geophysics 51, 123-136.

Chakravarthi, V., Sundararajan, N. 2004. Ridge regression algorithm for gravity inversion of fault structures with variable density. Geophysics 69, 1394–1404.

Chakravarthi, V., Sundararajan, N. 2005. Gravity modeling of 21/2-D sedimentary basins-a case of variable density contrast. Computers and Geosciences 31, 820–827.

Chakravarthi, V., Sundararajan, N. 2006. Gravity anomalies of multiple prismatic structures with depth-dependent density – A Marquardt inversion. Pure and Applied Geophysics 163, 229–242.

Chakravarthi, V., Sundararajan, N. 2007. Marquardt optimization of gravity anomalies of anticlinal and synclinal structures with prescribed depth-dependent density. Geophysical Prospecting 55, 571–587.

Chakravarthi, V., Sundararajan, N. 2008. TODGINV—A code for optimization of gravity anomalies due to anticlinal and synclinal structures with parabolic density contrast. Computers & Geosciences 34, 955–966.

Chua, L.O., Yang, L. 1988. Cellular neural networks. Theory. IEEE Trans Circuits Syst 35,1257–1272.

Eshaghzadeh, A., Kalantari, R.A. 2015. Anticlinal Structure Modeling with Feed Forward Neural Networks for Residual Gravity Anomaly Profile, 8th congress of the Balkan Geophysical Society DOI: 10.3997/2214-4609.201414210.

Eshaghzadeh, A., Hajian, A. 2018. 2-D inverse modeling of residual gravity anomalies from Simple geometric shapes using Modular Feed-forward Neural Network, Annals of Geophysics. 61,1, SE115.

Eslam, E., Salem, A., Ushijima, K. 2001. Detection of cavities and tunnels from gravity data using a neural network. Explor. Geophys 32, 204–208.

Essa, K.S. 2007. A simple formula for shape and depth determination from residual gravity anomalies. Acta Geophysica 55/2, 182–190.

Gerkens, A.J.C. 1989. Foundation of exploration Geophysics Elsevier.

Gupta, O.P. 1983. A least-squares approach to depth determination from gravity data. Geophysics 48, 357-360.

Hajian, A.R. 2004. Depth estimation of gravity data by neural network, M. Sc. thesis, Tehran University, Iran (unpublished).

Hammer. S. 1974. Graticule spacing versus depth discrimination in gravity interpretation. Geophysics 42, 60-65.

Kaftan, I., Salk, M., Şenol, Y. 2011. Evaluation of gravity data by using artificial neural networks case study: Seferihisar geothermal area (Western Turkey). Journal of Applied Geophysics 75, 711-718.

Last, B. J., Kubik, K. 1983. Compact gravity inversion. Geophysics 48, 713-721.

Lines, L.R., Treitel, S. 1984. A review of least-squares inversion and its application to geophysical problems. Geophys. Prosp 32, 159-186.

Marquardt, D.W. 1963. An algorithm for least-squares estimation of nonlinear parameters. Journal of the Society of Indian Applied Mathematics 11, 431–441.

Mohan, N.L., Anandababu, L., Rao, S. 1986. Gravity interpretation using the Melin transform, Geophysics 51, 114-122.

Nagy, D. 1966. Gravitational attraction of a right rectangular prism. Geophysics 31, 362–371.

Odegard, M.E., Berg, J.W. 1965. Gravity interpretation using the Fourier integral. Geophysics 30, 424-438.

Osman, O., Muhittin, A.A., Uçan, O.N. 2006. A new approach for residual gravity anomaly profile interpretations: Forced Neural Network (FNN). Ann. Geofis 49, 6.

Osman, O., Muhittin, A.A., Uçan, O.N. 2007. Forward modeling with Forced Neural Networks for gravity anomaly profile. Math. Geol 39, 593-605.

Plouff, D. 1976. Gravity and magnetic fields of polygonal prisms and application to magnetic terrain corrections. Geophysics 41, 727–741.

Salem, A., Ravat, D., Johnson, R., Ushijima, K. 2001. Detection of buried steel drums from magnetic anomaly data using a supervised neural network. J. Environ. Eng. Geophys 6,115-122.

Saxov, S., Nygaard, K. 1953. Residual anomalies and depth estimation. Geophysics 18, 913-928.

Sharma, B., Geldart, L.P. 1968. Analysis of gravity anomalies of two-dimensional faults using Fourier transforms. Geophys. Prosp 77-93.

Shaw, R.K., Agarwal, N.P. 1990. The application of Walsh transforms to interpret gravity anomalies due to some simple geometrically shaped causative sources: A feasibility study. Geophysics 55, 843-850.

Talwani, M. 1965. Computation with the help of a digital computer of magnetic anomalies caused by bodies of arbitrary shape. Geophysics 30,797–817.

Talwani, M., Ewing, M. 1960. Rapid computation of gravitational attraction of 3D bodies of arbitrary shape. Geophysics 25, 203–225.